Measurements and Modeling of Air Plasma Radiation in the VUV

Sean Mcguire, Carolyn Jacobs, Pierre Bruno Mariotto, Corentin Grimaldi, Augustin Tibère-Inglesse, Christophe O Laux

Measurements and Modeling of Air Plasma Radiation in the VUV

Sean D. McGuire*, Carolyn Jacobs†,Pierre B. Mariotto‡, Corentin H.C. Grimaldi§, Augustin Tibère-Inglesse¶, Christophe O. Laux‖
Laboratoire EM2C, CNRS UPR288, CentraleSupélec, Université Paris Saclay, 3 rue Joliot-Curie, Gif-sur-Yvette, France

Measurements of high temperature air emission spectra between 150 - 250 nm (VUV/UV) are presented. These measurements are calibrated in absolute intensity. The high temperature air was produced using an atmospheric pressure plasma torch facility. The centerline temperature of the plasma jet is approximately 6700 K. A VUV emission spectroscopy system was adapted to the plasma torch facility to acquire spectra from 150 to 250 nm. Absolute intensity spectra were obtained in this wavelength range. They were compared with numerical predictions of the line-by-line spectroscopy code SPECAIR. The overall agreement between the SPECAIR predictions and measurements is good, particularly above 180 nm. Several modifications to the SPECAIR radiation code were carried out in order to improve agreement with experiments. These modifications significantly improved agreement though, at lower wavelengths, the data indicate that a source of emission remains unaccounted for by SPECAIR. Several possibilities for this missing source of emission are discussed, including photodissociation of the nitric oxide molecule.

*Assistant Professor, Laboratoire EM2C, CNRS, CentraleSupélec, Université Paris-Saclay
†Current post: Lecturer, School of Mechanical and Mining Engineering, The University of Queensland, Brisbane St Lucia, QLD 4072, Australia
‡Doctoral Student, Laboratoire EM2C, CNRS, CentraleSupélec, Université Paris Saclay
§Doctoral Student, Laboratoire EM2C, CNRS, CentraleSupélec, Université Paris Saclay
¶Postdoctoral Researcher, Laboratoire EM2C, CNRS, CentraleSupélec, Université Paris Saclay
‖Professor, Laboratoire EM2C, CNRS, CentraleSupélec, Université Paris-Saclay

Nomenclature

$A_{\nu'\nu''}$	=	Einstein coefficient for spontaneous emission between vibrational states ν' and ν''
E_H	=	ionization energy of the hydrogen atom
E_∞	=	ionization energy of the radiating atom
E_i	=	excited state energy of radiating state
$\overline{R}$	=	average radius of electron orbit as defined and used by Griem (Ref. [1])
$R_e^{\nu'\nu''}$	=	electronic-vibrational transition moment between vibrational states ν' and ν''
S	=	total spin of electrons
X_p	=	mole fraction of species $'p'$
a_o	=	Bohr radius
c	=	speed of light
e	=	absolute value of electron charge
$f_{\nu'\nu''}^{abs}$	=	absorption oscillator strength between vibrational states ν' and ν''
$f_{\nu'\nu''}^{emis}$	=	emission oscillator strength between vibrational states ν' and ν''
h	=	Planck constant
l_i	=	orbital angular momentum quantum number (individual electron)
k	=	boltzmann constant
m_e	=	mass of electron
p	=	pressure
T	=	temperature
$\Delta\lambda_{Doppler}$	=	doppler broadening linewidth
$\Delta\lambda_{vdw}$	=	Van der Waals linewidth
Λ	=	projection of the total orbital angular momentum of a molecular electronic state
δ_{ij}	=	Kronecker delta function
λ	=	wavelength
ν	=	frequency
ν'	=	vibrational quantum number of upper state
ν''	=	vibrational quantum number of lower state
$\overline{\nu}_{\nu'\nu''}$	=	wavenumber of vibrational transition calculated according to r-centroid approximation
ψ_ν	=	vibrational wavefunction associated with vibrational state ν
$\hbar$	=	$h/2\pi$

superscripts

$'$	=	upper state involved in an optical transition
$''$	=	lower state involved in an optical transition

I. Introduction

High temperature air radiation is important for the design of spacecraft heat shields. Radiative codes are required to accurately estimate the radiative heat flux. As a general rule, the radiative heat flux becomes important at high entry velocities and for large capsule sizes. Johnston *et al* estimate that, for a 1-m radius sphere entering at 15 km/s (Mars return case), the radiative heat flux accounts for more than 85% of the total heat flux (see Fig. 1 of their paper) [2]. High entry velocities lead to high shock layer temperatures which lead to high levels of atomic and photoionization

radiation. Furthermore, these high temperatures lead to large contributions from the UV and VUV spectral regions to the total radiative heat flux [2, 3]. At lower entry velocities, the convective heat flux generally dominates. Emission from molecular species becomes more important for the calculation of the radiative heat flux. Beyond calculation of the radiative heat flux for reentry missions, radiative codes are necessary for analyzing emission and absorption spectra collected in ground testing facilities. Such an analysis provides information about the temperature and chemical composition of the gas, which can then be used to validate hydrodynamic codes or chemical kinetic models. For these reasons, a lot of work has focused on the development and validation of radiative codes. An article by Zammit *et al* provides a recent example looking at modeling of high temperature air radiation [4].

The work in this paper addresses two goals. The first goal is to measure equilibrium air emission in the VUV for conditions relevant for atmospheric entry. The second goal is to compare with radiative code predictions in order to assess and improve model performance in this spectral zone. The radiative code SPECAIR will be used in this paper [5, 6]. The work presented in this article was done with the CentraleSupélec plasma torch facility, which has the advantage of producing air plasmas in local Thermodynamic Equilibrium (LTE) at temperatures up to 7000 K and atmospheric pressure. The measured spectra provide an excellent means for validating radiative models because the thermochemical state of the plasma is well known.

II. Measurements

The facility used to produce the plasma for the emission studies is a TAFA Model 66 inductively coupled plasma (ICP) torch powered by a 120 kVA radio frequency LEPEL Model T-50-3 power supply. The power supply operates at 4 MHz and provides a maximum of 12 kV DC and 7.5 A to the oscillator plates. Details of the plasma torch facility may be found in previous publications [7, 8]. The plasma at the exit of the torch is at atmospheric pressure. Figure 1 shows a schematic of the facility. For the experiments presented here, a 5-cm diameter exit nozzle was used.

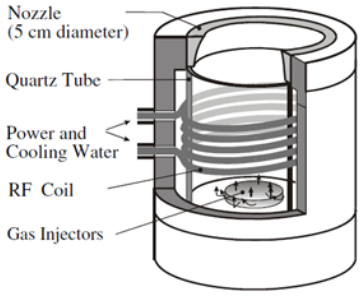

Fig. 1 Plasma torch head and nozzle assembly. The gas injectors include radial, swirl and axial injectors.

The temperature profile of the plasma jet was obtained by measuring the absolute emission from the oxygen triplet at 777 nm. This is done using a visible spectrometer (Acton SpectraPro 500i), imaging setup and a calibrated Tungsten ribbon lamp (Optronics Laboratories OL550). A filter is installed in the optical path to suppress higher

order interferences within the spectrometer. The imaging system for the visible wavelength spectrometer makes use of parabolic mirrors and a periscope to image the spectrometer slit across the jet profile. Intensity measurements are Abel-inverted to provide spatially resolved intensity profiles. The procedure for these emission-based temperature measurements is documented in several references [5, 7, 9]. The analysis relies upon the assumption of thermochemical equilibrium - an assumption that has been previously verified using this plasma torch facility with air injection [5, 7]. Figure 2a shows the temperature profile for the conditions studied here. Given this temperature profile, the composition of the air plasma may be calculated using NASA CEA [9] and is shown in Fig. 2b. Based on previous work, it is known that the *NO* bands are responsible for a large portion of the VUV/UV air emission at these conditions [5, 7].

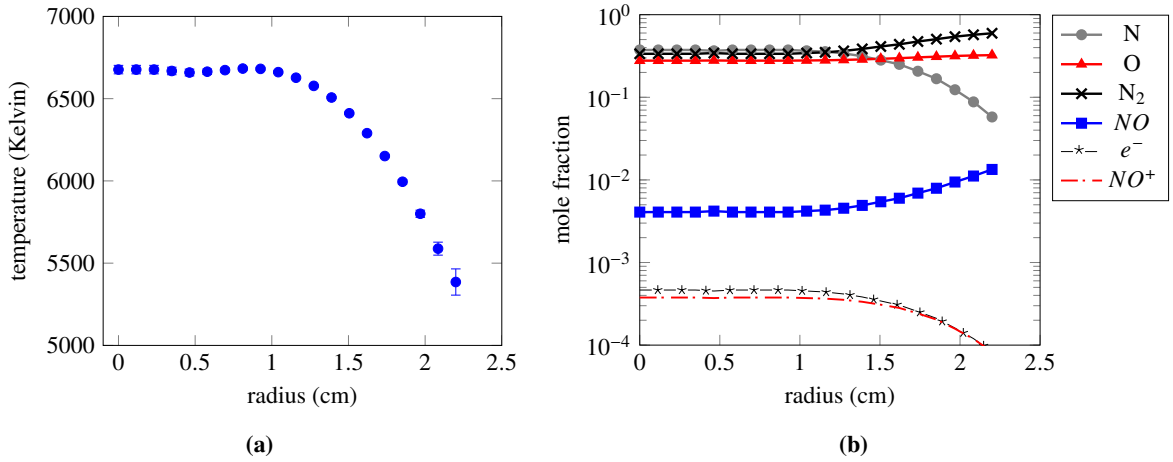

Fig. 2 a) Temperature profile obtained by measuring the 777 nm oxygen triplet emission. The error bars are small, indicating that the temperature is accurately known. b) Composition of the plasma jet as a function of radius based upon the measured temperature profile. Ar**,** CO **and** C **are present in mole fractions on the order of** 6×10^{-3}**,** 2×10^{-4} **and** 6×10^{-5}**, respectively.**

The VUV measurements are a continuation of work begun several years back using a nitrogen purged VUV spectrometer [10]. Then, measurements were obtained down to 170 nm, but oxygen absorption was affecting the measurements below a wavelength of about 180 nm, making it somewhat difficult to compare with radiative model predictions. For this work, a McPherson vacuum spectrometer is used that is capable of making measurements down to 120 nm. The setup is identical to the system used in Ref. [11], where VUV/UV emission from carbon monoxide was studied. A slightly modified setup was used to make VUV measurements in a recombining nitrogen plasma [12]. Figure 3 shows a diagram of the VUV system. An imaging box with two mirrors (Acton optics with a #1200 coating for 120 nm reflection) is attached to the spectrometer for imaging the spectrometer slit onto the plasma. An adapting tube protrudes from this imaging box and terminates at the plasma boundary to avoid absorption by the O_2 Schumann-Runge in ambient air (Fig. 3b). This tube is specially designed to withstand the thermal heat flux coming from the hot plasma. The final piece in contact with the plasma is a water-cooled copper piece. Teflon and PEEK plastics are used in the portion of tube separating this copper adaptor from the imaging box. These plastics were chosen for electrical isolation

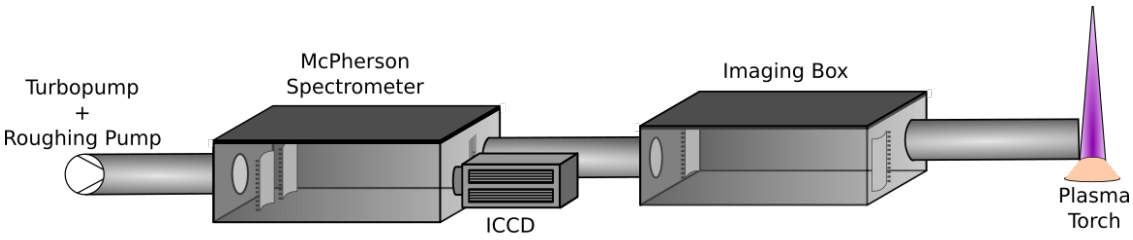

(a) Spectroscopic system used for making spectrally resolved VUV measurements of air emission.

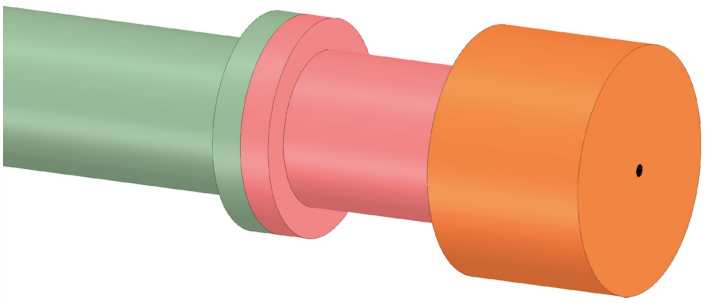

(b) Detail of the tube that protrudes from the imaging box and extends the optical line to the plasma. The final portion in orange touches the boundary of the plasma jet - it is manufactured out of copper and is water cooled. A 2 mm hole provides optical access. The portion in red is manufactured out of Teflon. Both the red and orange sections - which together makeup the final 10 cm of the optical path - are put under an argon purge. The portion in green is manufactured out of PEEK plastic and is put under vacuum. A MgF_2 window separates the vacuum section from the argon purge section.

Fig. 3

given that the plasma is at a 10 kV floating potential. Most of the system is placed under vacuum ($< 10^{-3}$ Torr). However, the final portion of the optical setup which is in contact with the torch is placed under an argon purge (see Fig. 3b for a detail of this part). A continuous argon purge was run at a pressure slightly above 1 atm to prevent oxygen from leaking into the system. Pressure relief ports were drilled in the teflon piece to permit a portion of the argon to exit via these holes, rather than entirely into the plasma. The remaining portion exited through the final viewing hole, directly entering the plasma jet. Our measurements indicate that this purge did not affect the measured radiation. All measurements above 200 nm agreed very well with SPECAIR predictions and SPECAIR has already been validated in this spectral region. Ref. [11] details additional tests performed on an alternate CO_2/Ar mixture.

For calibration, an argon discharge supplies radiation traceable to NIST standards in the VUV/UV spectral regions [13]. The adapting arm linking the imaging box to the plasma was replaced with a separate adaptor for these measurements so that the argon discharge was located at the system focus. A diaphragm was used to limit the aperture of the imaging setup and to ensure that the same aperture was used for both the calibration and plasma torch measurements. Finally, due to high levels of stray light during the calibration measurement, a VUV transmission filter (eSource Optics 50150FBB) was installed for the calibration measurements. The spectrally resolved transmission of this filter was known

and verified by performing calibrations both with and without the filter. For spectral regions where it was possible to compare the two calibrations, the measurements reproduced the quoted transmission profile. This transmission filter was not used in the plasma torch measurements where stray light was not a problem. An identical procedure was used in McGuire *et al* [11].

For all emission measurements, a VUV compatible PI-MAX2 camera from Princeton Instruments was used. The raw measurements were therefore images, with one axis corresponding to wavelength and the second axis corresponding to plasma jet radius. To produce the final spectra, the zone along the spatial axis corresponding to the center of the plasma jet was first identified. The images were then binned across this zone to produce a spectrum. The same binning was also applied to stray light measurements, which were obtained by tuning the spectrometer to 120 nm where no signal was observed. The resulting stray light signal was subtracted from all spectra. Finally, any residual background due to dark current was also subtracted. This dark current was determined by registering the signal in zones where no light is incident on the camera due to the spectrometer design. This same procedure was applied to obtain calibration spectra. Multiplying the emission spectra in the torch by the calibration spectra produced the final spectra, calibrated in absolute intensity.

The intensity of the measured VUV/UV emission is a product of two measurements: the signal recorded in the torch and the calibration factor. Each of these factors has a corresponding uncertainty. δU_{calib} and δU_{signal} denote the relative uncertainty in the calibration and the signal recorded in the torch, respectively. Assuming these two errors to be uncorrelated, the relative uncertainty in the intensity is given by $\delta U_{intensity} = \sqrt{\delta U_{calib}^2 + \delta U_{signal}^2}$ (where $\delta U_i = \Delta U_i / U_i$ and ΔU_i is the absolute uncertainty in U_i). The dominant source of uncertainty comes from the calibration signal. The reported intensity curve is a smooth function. However, the measurements indicate that this intensity fluctuates slightly with wavelength. These fluctuations are less than 5% of the measured amplitude across the measured wavelength range. The only other known source of uncertainty is the camera dark current signal, but this is negligible in comparison. Therefore, the relative uncertainty in the absolute intensity of the final measurements is taken to be less than 5% across the entire wavelength range.

The slit function for the VUV/UV measurements is shown in Fig. 4. The VUV system provides line-of-sight measurements along the chord intersecting the plasma centerline, 2.5 cm downstream of the nozzle exit. The aforementioned temperature measurements are performed at the same vertical/axial location. Figure 5 shows the measured VUV spectrum calibrated in absolute intensity.

III. Modeling - SPECAIR radiation code

Radiation modeling for comparison with measurements was done using the radiation code SPECAIR [5, 6]. The initial SPECAIR model for the nitric oxide bands was developed in Refs. [7, 14, 15] to include important transitions in the VUV such as the delta and epsilon systems that had not been previously considered in high temperature air radiation

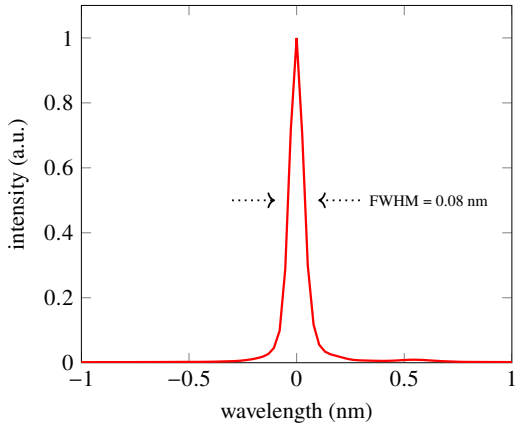

Fig. 4 Measured slit function of the VUV system.

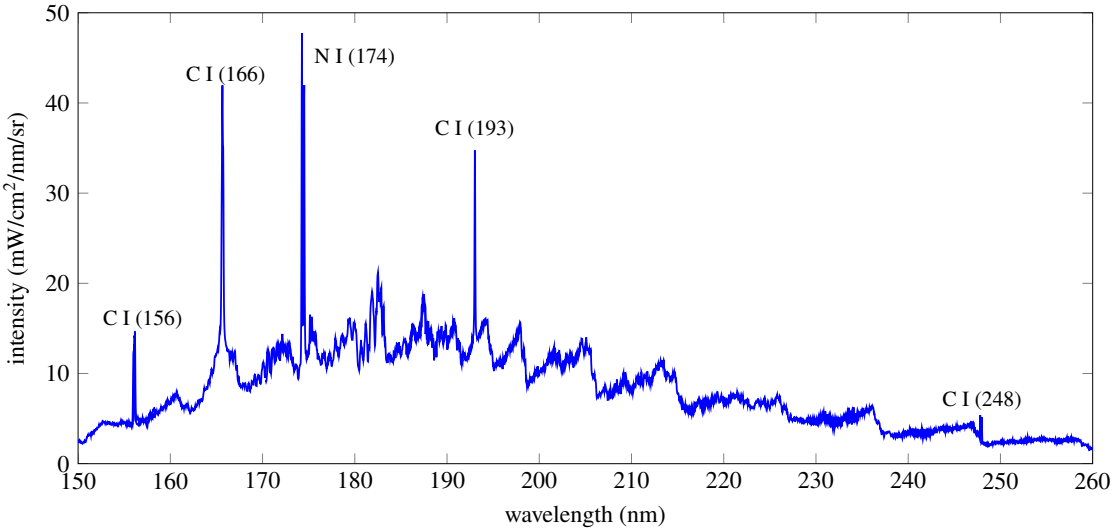

Fig. 5 Measured spectrum from the high temperature air produced by the plasma torch. Several atomic carbon lines are observed due to the presence of carbon dioxide in the air.

models. The model was then updated in Ref. [5] to account for line position perturbations in transitions involving the $^2\Pi$ states. This SPECAIR model was found to give very good agreement with measurements for wavelengths above 200 nm. This code was modified for this work to improve agreement at lower wavelengths. The next two sub-sections discuss the modeling of molecular and atomic emission, respectively. For each molecular system or atomic feature, the original SPECAIR model is presented, followed by any updates that were incorporated into the model as a result of this work.

A. Molecular Emission - nitric oxide bands

The measured molecular emission comes primarily from nitric oxide systems. For a generic band system, the Einstein coefficients included in SPECAIR are calculated using the method outlined in Laux and Kruger [7, 14], which yields the following equation:

$$A_{\nu'\nu''} = \frac{64\pi^4\nu^3}{3hc^3}\,\frac{(2-\delta_{0,\Lambda'+\Lambda''})}{(2-\delta_{0,\Lambda'})}\,(R_e^{\nu'\nu''})^2 \tag{1}$$

where:

$$(R_e^{\nu'\nu''})^2 = \left[\int_0^\infty \psi_{\nu'}(r)\,Re(r)\,\psi_{\nu''}(r)dr\right]^2 \tag{2}$$

$R_e^{\nu'\nu''}$ is the electronic-vibrational transition moment, $\psi_{\nu'}$ and $\psi_{\nu''}$ represent the vibrational wavefunctions of the upper and lower states respectively, Λ' and Λ'' represent the projection of the orbital angular momentum of the upper and lower states respectively and $\delta_{i,j}$ is the Kronecker delta function. The above expressions are taken from Schadee [16] and CGS units are used. These lead to a set of equations linking the square of the electronic-vibrational transition moment $(R_e^{\nu'\nu''})^2$ to other conventional values as follows:

$$\begin{aligned}
A_{\nu'\nu''} &= \frac{64\pi^4\nu^3\left(2-\delta_{0,\Lambda'+\Lambda''}\right)}{3hc^3\left(2-\delta_{0,\Lambda'}\right)}(R_e^{\nu'\nu''})^2 = \left(2.026\times10^{-6}\right)(\overline{\nu}_{\nu'\nu''})^3\,\frac{2-\delta_{0,\Lambda'+\Lambda''}}{2-\delta_{0,\Lambda'}}\left(\frac{R_e^{\nu'\nu''}}{ea_o}\right)^2 \\
f_{\nu'\nu''}^{abs} &= \frac{8\pi^2 m_e\nu\left(2-\delta_{0,\Lambda'+\Lambda''}\right)}{3he^2\left(2-\delta_{0,\Lambda''}\right)}(R_e^{\nu'\nu''})^2 = \left(3.0376\times10^{-6}\right)\overline{\nu}_{\nu'\nu''}\,\frac{2-\delta_{0,\Lambda'+\Lambda''}}{2-\delta_{0,\Lambda''}}\left(\frac{R_e^{\nu'\nu''}}{ea_o}\right)^2 \\
f_{\nu'\nu''}^{emis} &= \frac{2-\delta_{0,\Lambda''}}{2-\delta_{0,\Lambda'}}f_{\nu'\nu''}^{abs} \\
\sum(R_e^{\nu'\nu''})^2 &= \left(2-\delta_{0,\Lambda'+\Lambda''}\right)(2S+1)\,(R_e^{\nu'\nu''})^2
\end{aligned} \tag{3}$$

where $\sum(R_e^{\nu'\nu''})^2$ represents the sum of the electronic-vibrational transition moment across all electronic subtransitions. The above equations hold as long as the electronic-vibrational transition moment $R_e(r)$ has been calculated according to the convention of Whiting *et al* [17]. In the above expressions, $h = 6.626\times10^{-27}$ erg·s, $c = 3.00\times10^{10}$ cm/s, $e = 4.803\times10^{-10}$ statC, $m_e = 9.11\times10^{-28}$ g, $a_o = 5.291\times10^{-9}\ cm$ (Bohr radius), ν is the frequency in Hz, $\overline{\nu}_{\nu'\nu''}$ is the wavenumber of the transition in cm^{-1} and $R_e^{\nu'\nu''}$ is in atomic units (multiple of ea_0). Λ' and Λ'' are the projected orbital angular momentum quantum numbers of the upper and lower states respectively. Meanwhile, the Hönl-London factors are calculated using the method of Whiting *et al* [17]. These are then used along with the Einstein coefficients to determine the line strength of a specific rovibrational transition.

For calculations of the Einstein coefficients for molecular band systems that are not impacted by perturbations, the Rydberg-Klein-Rees (RKR) method is first used to determine the potential energy curves for the relevant electronic states. The vibrational wavefunctions are then calculated and used, along with the electronic-vibrational transition moment function taken from the literature, to calculate a set of Einstein coefficients for a given band system. This is the approach used for the γ, ϵ and β' systems of NO. Table 1 shows the sources and values used for these calculations. This methodology does not take into account perturbations between quantum states. The wavefunctions of states perturbed by

Table 1 Sources for the parameters used in the RKR portion of the *NO* molecular emission calculations from the A, D and B' upper states to the X lower state.

State	Molecular Constants	Diss. Energy (cm^{-1})
X $^2\Pi_r$	Amiot [18]	Lavrov [19]
A $^2\Sigma^+$	Huber and Herzberg [20]	Lavrov [19]
D $^2\Sigma^+$	Huber and Herzberg [20]	Lavrov [19]
B' $^2\Delta$	Huber and Herzberg [20]	Lavrov [19]

avoided crossings assume a hybrid form, characterized by a mixture of the quantum states involved in the perturbation. This is the case for emission from excited $^2\Pi$ states of *NO* and the methodology for these systems will be detailed below.

Emission from *NO* $^2\Sigma^+$ states: The $\gamma(A^2\Sigma^+ - X^2\Pi)$ and $\epsilon(D^2\Sigma^+ - X^2\Pi)$ are modeled using the approach outlined above - no perturbations were taken into account. The ETMF of Langhoff, Bauschlicher and Partridge was used for the *NO* γ system emission [21]. The ETMF for the *NO* ϵ system was also taken from calculations done by Langhoff and co-workers [22]. Emission from vibrational levels up to $v = 8$ in the A-state and $v = 5$ in the D-state are accounted for.

In this paper, the maximum vibrational level of the D-state was increased from $v = 5$ to $v = 6$. Figure 6a shows the effect of this modification on the SPECAIR calculation, which is minor and limited to wavelengths below 175 nm.

The *NO* γ' ($E^2\Sigma^+$ - $X^2\Pi$) system is included in SPECAIR as discussed in Ref. [7]. The electronic transition dipole moment used was that of De Vivie and Peyerimhoff [23]. The spectroscopic constants for the $E^2\Sigma^+$ state were taken from Huber and Herzberg [20]. The resulting calculations largely overpredict the measured photoabsorption cross-sections reported by Chan, Cooper and Brion [24] discussed in Section V. Furthermore, the impact of this system on the high temperature air emission spectrum was minimal. Appendix A contains figures that illustrate these points. For these reasons, this system is not included in the SPECAIR calculations shown below.

Emission from *NO* $^2\Delta$ states: Emission from the $\beta'(B'\,^2\Delta - X^2\Pi)$ was modeled using the standard approach and no perturbations were taken into account. The β' system primarily affects the spectrum at wavelengths below approximately 180 nm, and even then only weakly with an average magnitude less than 1 $mW/cm^2/nm/sr$. The ETMF for this band was taken from de Vivie and Peyerimhoff [23]. Emission from vibrational levels up to $v = 7$ in the B'-state are accounted for.

For this work, the maximum vibrational level of the B'-state was increased from $v = 7$ to $v = 9$. Figure 6b shows the effect of this modification on the SPECAIR calculation, which is negligible and limited to wavelengths below 160 nm.

The *NO* $F^2\Delta$ - $X^2\Pi$ system was also added to SPECAIR. As with the γ' system of *NO*, the resulting calculations largely overpredict the measured photoabsorption cross-sections reported by Chan, Cooper and Brion [24]. The corresponding impact on the high temperature air emission spectrum is also minimal. Appendix B contains figures that

illustrate these points. For these reasons, this system is not included in the SPECAIR calculations shown below.

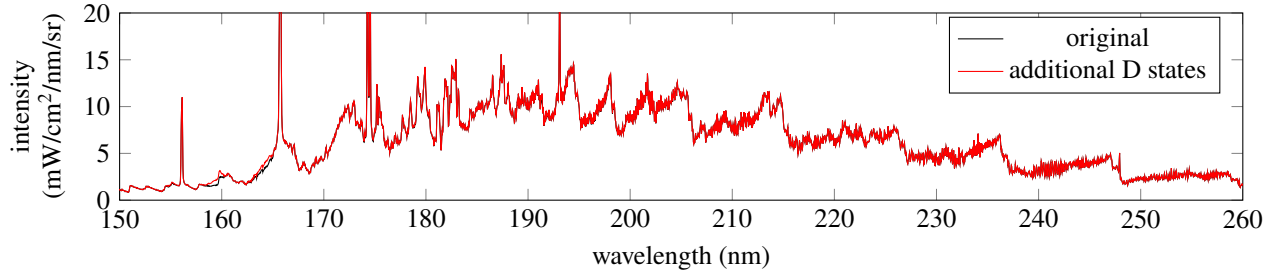

(a)

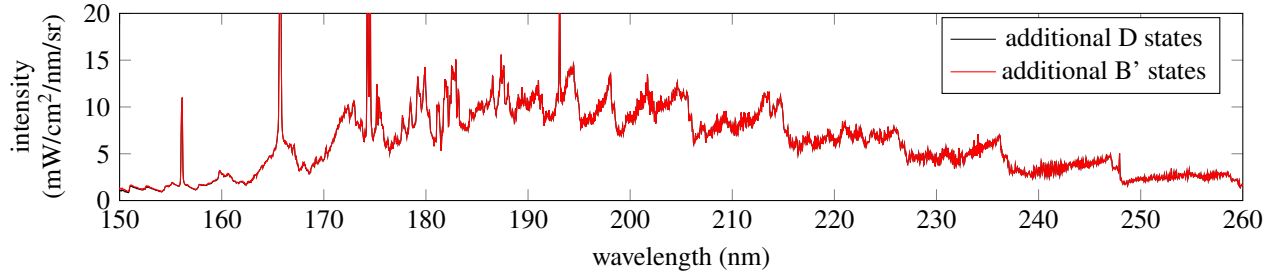

(b)

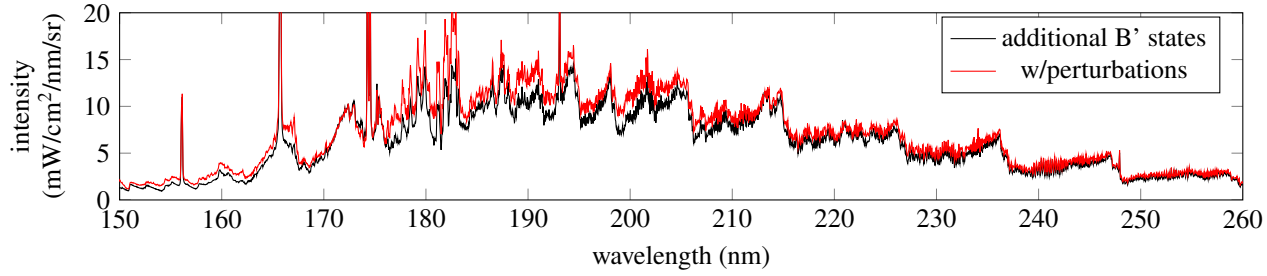

(c)

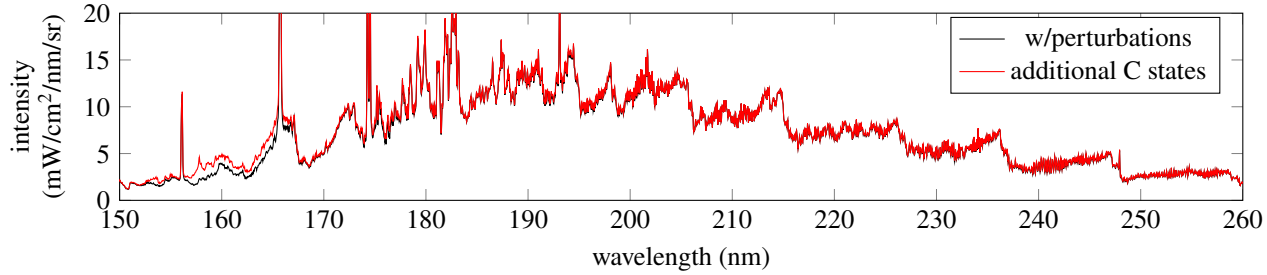

(d)

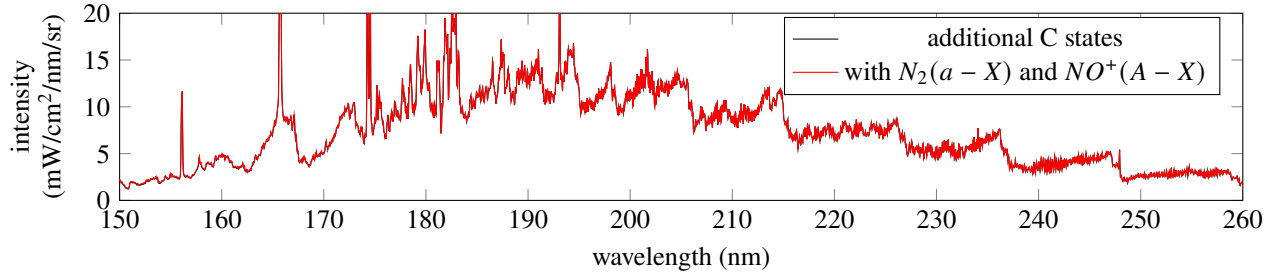

(e)

Fig. 6 Evolution in the SPECAIR calculation after several modifications. The modifications are made sequentially from subplots a) - e). Once a modification is made, it is preserved for the remaining subplots that follow.
a) The original SPECAIR and an initial update of the SPECAIR calculation. The curve "*additional D states*" is the same as the original calculation but with the maximum vibrational level of the D-state increased from $v = 5$ to $v = 6$.
b) The curve "*additional B' states*" is the same as the curve "*additional D states*" but with the maximum vibrational level of the B'-state increased from $v = 7$ to $v = 9$.
c) The curve "*w/perturbations*" is the same as the curve "*additional B' states*" but with the perturbation calculation for the oscillator strengths of the $^2\Pi$ states accounted for as described in the text.
d) The curve "*additional C states*" is the same as the curve "*w/perturbations*" but with the maximum vibrational level of the NO C-state increased from $v = 4$ to $v = 9$.
e) The curve "*with* $N_2(a-X)$ *and* $NO^+(A-X)$" is the same as the curve "*additional C states*" but with the N_2 $(a-X)$ and $NO+$ $(A-X)$ systems added.

Emission from *NO* $^2\Pi$ states: Perturbations amongst the various $^2\Pi$ states of *NO* have been noted in the literature [25, 26]. These perturbations affect both the line strength and position of individual lines within these systems. This paper uses the notation of Gallusser and Dressler [25] and SPECAIR accounts for emission from the $B^2\Pi - X^2\Pi$, $C^2\Pi - X^2\Pi$, $L^2\Pi - X^2\Pi$, $K^2\Pi - X^2\Pi$ and $Q^2\Pi - X^2\Pi$ systems. The primary $^2\Pi - {}^2\Pi$ transitions of *NO* contributing to the observed emission in the UV/VUV are the $B - X$ and $C - X$ systems, also known as the β and δ systems. These $^2\Pi - {}^2\Pi$ transitions require a special treatment because of the strong perturbations among the various $^2\Pi$ states of *NO*. These perturbations affect both the line positions and the line strengths. The original SPECAIR calculates the perturbed energies and line positions using the perturbation method outlined by Gallusser and Dressler. However, perturbations in the line strengths were not taken into account.* In this paper, SPECAIR was modified as follows:

- The maximum emitting vibrational level for the $C^2\Pi$ state was increased from $v_{max} = 4 \rightarrow 9$. This impacts emission from the *NO* δ system.
- Emission from the $L^2\Pi - X^2\Pi$, $K^2\Pi - X^2\Pi$ and $Q^2\Pi - X^2\Pi$ systems was accounted for.
- The effect of perturbations on the oscillator strength was accounted for the $B^2\Pi - X^2\Pi$, $C^2\Pi - X^2\Pi$, $L^2\Pi - X^2\Pi$, $K^2\Pi - X^2\Pi$ and $Q^2\Pi - X^2\Pi$ systems.

Note that the $^2\Pi$ states have a multiplicity of two. Each branch of the multiplet is impacted separately by the perturbation calculation of Gallusser and Dressler. The calculations in SPECAIR fully account for this separate dependence on the perturbed energy. However, as a first approximation, this separate dependence on the line strength is ignored. Rather, the oscillator strength for each branch of the multiplet is taken to be the average of the two branches. As a check on this assumption, we replaced the oscillator strength by the maximum or minimum of the two branches (rather than the average) to see what changes this resulted in and found the difference to be minimal.

As a result of these modifications, the SPECAIR calculations in this paper accounts for emission from vibrational levels up to $v = 9$ in the δ system, $v = 25$ in the β system, $v = 11$ in the L-X system, $v = 3$ in the Q-X system and $v = 4$ in the K-X system. Additionally, the effect of perturbations on the energy levels and on the oscillator strengths is accounted for. Figures 6c-6d show the effect of this modification on the SPECAIR calculation. In Fig. 6c, the perturbation on the energy levels and oscillator strengths is accounted for. In addition, the *NO* $L - X$, $K - X$ and $Q - X$ systems are added. However, the maximum vibrational quantum number of the C-state is limited to $v = 4$ as done in the original SPECAIR calculation, even though the perturbation calculations permit calculations up to $v = 9$. In Fig. 6d, the maximum vibrational quantum number is extended to $v = 9$. In comparing Figures 6c and 6d, it is apparent that increasing the maximum vibrational quantum number of the C-state from $v = 4$ to $v = 9$ has a very minimal impact. However, the impact of the perturbations on the oscillator strengths has a substantial impact.

*For a few vibrational levels, the perturbed line positions computed with the Gallusser and Dressler method were then replaced by the more accurate experimental line positions of Amiot and Verges [27] for the $v = 0$ level of the C-state and the $v = 7 - 10$ levels of the B-state, and of Imajo *et al* [28] for the $v = 1$ level of the C-state.

Emission from NO^+(A - X) and N_2(a-X): Two new electronic systems were added to SPECAIR: the NO^+ $A^1\Pi$ - $X^1\Sigma^+$ and N_2 $a^1\Pi_g - X^1\Sigma_g^+$ (Lyman-Birge-Hopfield) transitions. For the NO^+ $A^1\Pi$ - $X^1\Sigma^+$ system, the electronic transition dipole moment function of Partridge, Langhoff and Bauschlicher [29] was used (See Fig. 7 and Table 2 of their article). For the Lyman-Birge-Hopfield system of N_2, the magnetic dipole transition was modeled using the oscillator strengths reported by Pilling, Bass and Braun [30]. Figure 6e shows that the addition of these two systems has a negligible impact on the predicted emission.

Relative contribution from various systems: Figure 7 shows the contributions from various *NO* bands discussed above as well as other residual sources of the predicted emission calculated based on the temperature profile shown in Fig. 2a. The calculations in Fig. 7 were performed after updating SPECAIR as described in this section.

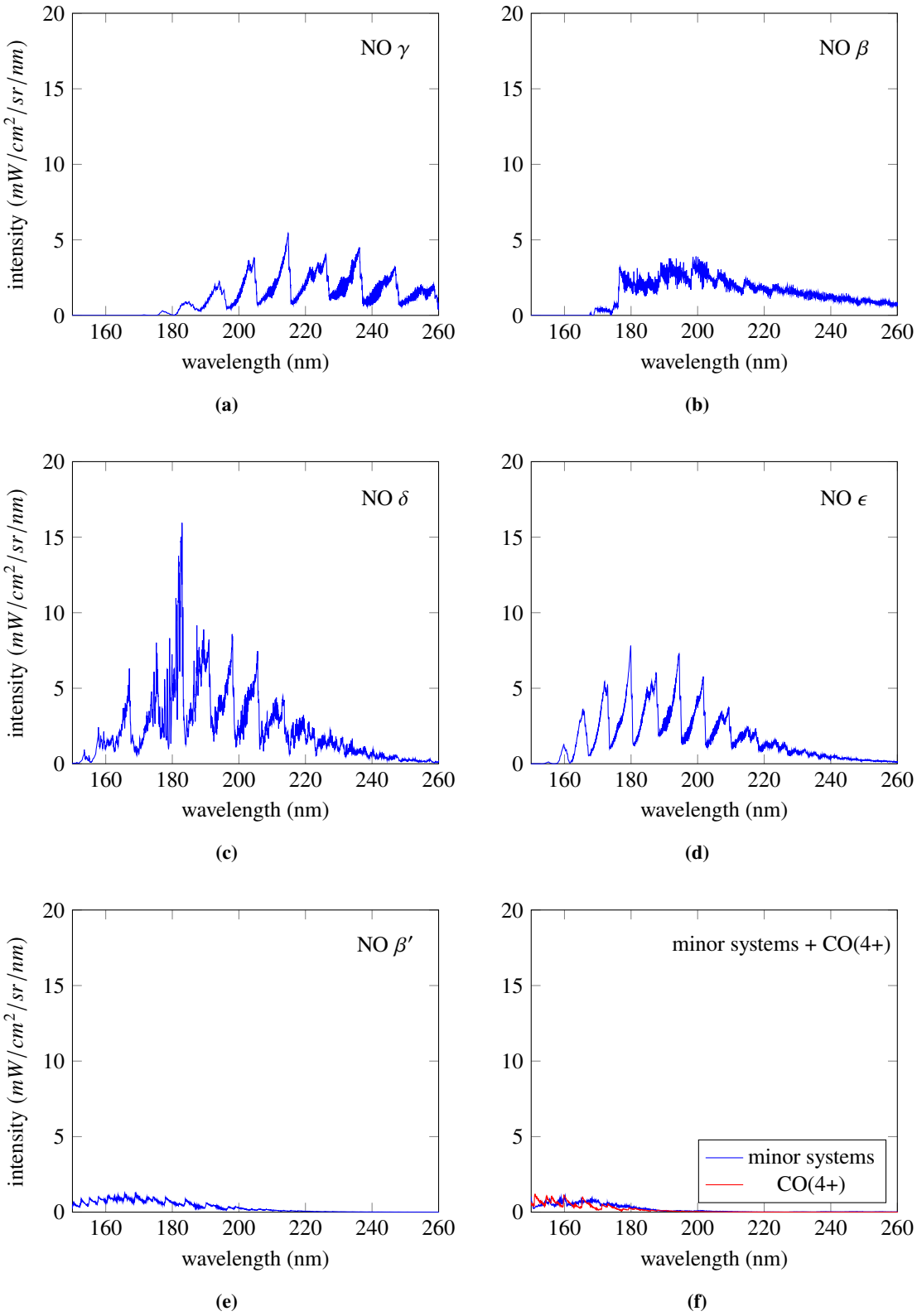

Fig. 7 Contributions to predicted SPECAIR emission using the temperature profile in Fig. 2a. All calculations were made after SPECAIR was updated as described in Section III. Contributions from a) *NO* γ system, b) *NO* β system, c) *NO* δ system, d) *NO* ϵ system, e) *NO* β' system and f) the curve labeled CO(4+) contains emission from the CO 4+ system while the curve labeled 'minor systems' contains the combined emission from N_2 $a^1\Pi_g$ - $X^1\Sigma_g^+$, *NO*+ $A^1\Pi$ - $X^1\Sigma^+$, *NO* $L^2\Pi - X^2\Pi$, *NO* $K^2\Pi - X^2\Pi$ and *NO* $Q^2\Pi - X^2\Pi$ systems.

B. Atomic Emission - 174 nm feature

The atomic nitrogen feature at 174 nm is optically thick for the conditions studied (see Fig. 8). To account for the extreme self-absorption along the line-of-sight and correctly predict the measured intensity, it is necessary to correctly predict the lineshape. Line broadening mechanisms include Doppler, Stark, resonance, van der Waals and natural line broadening mechanisms. The dominant mechanism here is Doppler broadening, which is described by a Gaussian lineshape of full width at half maximum (FWHM) given by:

$$\Delta\lambda_{Doppler} = \lambda_{ul}\sqrt{\frac{8kT\ln 2}{mc^2}} \tag{4}$$

Calculations indicate the Van der Waals broadening is also important. Though the FWHM of the van der Waals broadening is smaller than that of the Doppler broadening, the lineshape falls off more slowly from line center due to the Lorentzian profile. Van der Waals broadening is estimated based upon the approach detailed by Griem [1, 31]. The following formula, adapted from Griem [1], was used for the Lorentzian FWHM of the nitrogen line:

$$\Delta\lambda_{vdw} = \sum_p \frac{\lambda^2}{c}\left(\sqrt{\frac{8kT}{\pi}}\right)^{3/5}\left(\frac{\hbar^5\overline{R^2}}{m_e^3}\right)^{2/5}\left(\frac{p}{kT}\right)\left(\frac{X_p}{E_p^{4/5}m_{rp}^{3/10}}\right) \tag{5}$$

where all values are in SI units. m_e is the mass of the electron, X_p the mole fraction of the perturber, E_p the energy of the first excited state of the perturber connected to its ground state by an allowed transition and m_{rp} the reduced mass of the radiator and the perturber. The formula for the parameter $\overline{R}$ is taken from Griem:

$$\overline{R^2} = \frac{1}{2}\frac{E_H}{E_\infty - E_i}\left[5\frac{E_H}{E_\infty - E_i} + 1 - 3l_i(l_i+1)\right] \tag{6}$$

where E_H is the ionization energy of the hydrogen atom, E_∞ is the ionization energy of the radiating atom and E_i is the excited state energy of the radiator. l_i is the orbital angular momentum quantum number of the radiating state. The FWHM calculated by Eqn. 5 for each perturber was increased by a multiplicative factor of $n_e^{2/5}$, where n_e is the number of valence electrons of the perturber. This is done based upon a remark by Griem in section 4.8 of his text [1]. The calculations above apply only to atom-atom collisions as discussed by Griem. However, they are nonetheless applied to the molecular N_2 perturber. While the results give good agreement, the value for the Van der Waals broadening should therefore be considered as approximate.

Tables 2 and 3 show the parameters used in Eqn. 6 for the van der Waals calculation. For conditions near the center of the plasma jet (T = 6700 K, p = 1 atm), Doppler broadening is calculated to have a FWHM (full-width at half maximum) of 2.3 pm whereas van der Waals broadening is calculated to have a FWHM of 0.3 pm.

Table 2 Parameters used in Eqn. 6 for the line broadening calculation for the 174 nm line.

$E_H\ (eV)$	$E_\infty\ (eV)$	$E_i\ (eV)$	l_i
13.6	14.5	10.7	0

Table 3 Species-specific parameters used in Eqn. 6 for the line broadening calculation for the 174 nm line. n_e is the number of valence electrons taken for the particular perturber. The value of $n_e = 10$ for N_2 is twice the value for an individual N atom. E_p for N_2 corresponds to the energy of the $b^1\Pi_u$ state which is the first electronic state connected to the ground state by a dipole allowed transition.

	X_p	$E_p\ (eV)$	n_e
N	0.31	10.3	5
O	0.29	9.1	6
N_2	0.39	12.6	10

IV. Results

Figure 8 shows a SPECAIR calculation of equilibrium air emission corresponding to the measured temperature profile in Fig. 2a. The radiative transfer equation is solved along the line-of-sight to yield the calculated spectrum. The uncertainty in the measured temperature profile (Fig. 2a) leads to a corresponding uncertainty in the calculated intensity profile. This uncertainty is less than 5% across the entire wavelength range and, for wavelengths above 160 nm, is less than 3%. Prominent atomic features include the 174 nm atomic lines of nitrogen as well as three atomic carbon lines at 156 nm, 166 nm and 193 nm. The molecular structure is primarily composed of nitric oxide molecular bands: the $\gamma(A^2\Sigma^+ - X^2\Pi)$, $\beta(B^2\Pi - X^2\Pi)$, $\delta(C^2\Pi - X^2\Pi)$, $\epsilon(D^2\Sigma^+ - X^2\Pi)$, $\beta'(B'^2\Delta - X^2\Pi)$ systems. The molecular bands of *NO* are not heavily optically thick in Fig. 8. The difference in intensity between the calculations of *NO* emission with and without self-absorption is very small over a large portion of the spectrum and is maximal around 180 nm where the difference grows to a factor of 2. The primary effect of self-absorption is on the atomic lines such as the nitrogen feature at 174 nm, which is optically thick. Figure 9a shows a comparison between the experimental results and the original SPECAIR calculation, after convolving with the measured slit function. Figure 9b shows a comparison between experimental results and the updated SPECAIR calculation after convolving the SPECAIR calculation in Fig. 8 with the measured slit function. The updates to the SPECAIR calculation significantly improve the agreement with the experiment at wavelengths below 200 nm.

The agreement between the updated SPECAIR calculation and the experiment is quite good down to approximately 180 nm. The amplitude of the nitrogen feature at 174 nm - which is very sensitive to line broadening estimates because of strong self-absorption - appears to be well predicted. Below 180 nm, SPECAIR is found to underpredict the observed molecular structure of the spectrum. This suggests that sources of emission are missing in the SPECAIR calculation.

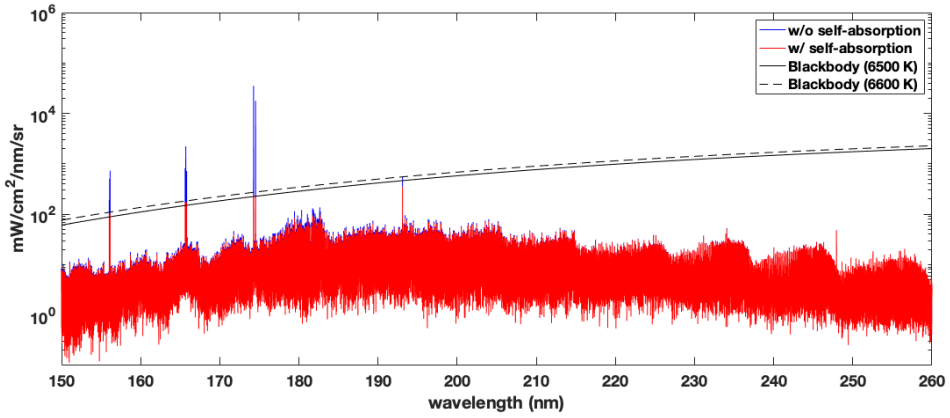

Fig. 8 SPECAIR calculation based upon the temperature profile in Fig. 2a. Two blackbody curves are included for reference.

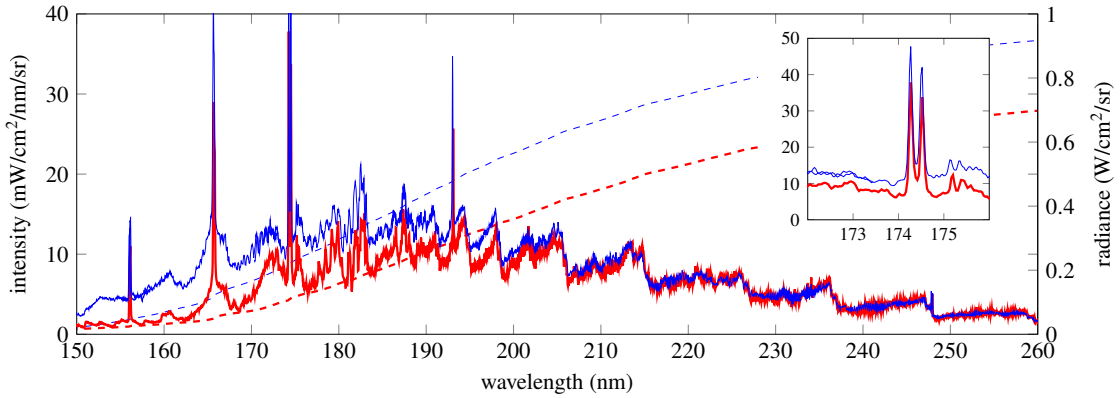

(a)

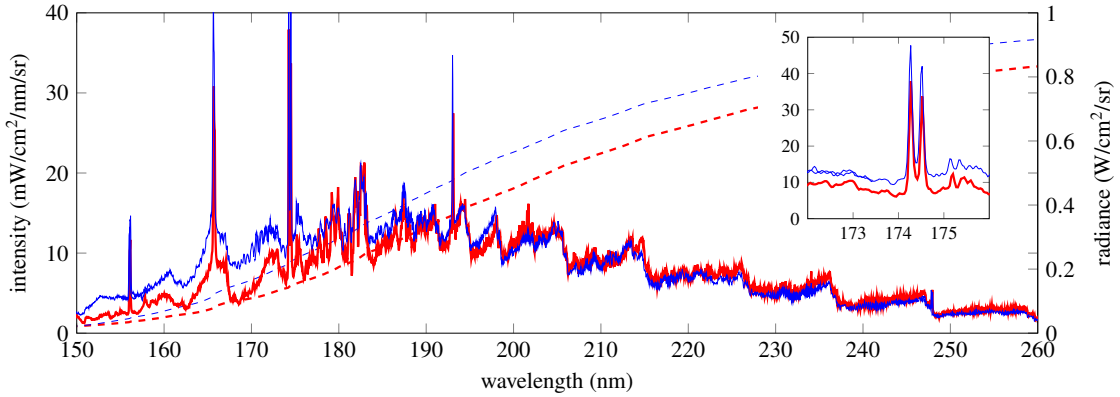

(b)

Fig. 9 a) Comparison between experiment (blue) and original SPECAIR calculation (red). b) Comparison between experiment (blue) and updated SPECAIR calculation (red).

V. Discussion

Despite the good agreement between the SPECAIR calculation and experiment, small discrepancies remain. The goal of this section is to discuss potential sources of this disagreement.

A. SPECAIR comparison with low temperature photoabsorption data

Chan *et al* [24] used electron energy loss spectroscopy to measure photoabsorption cross-sections from nitric oxide. In their experiments, *NO* was taken from a compressed cylinder and would have been essentially at or close to room temperature. In 2007, Kato *et al* [32] performed another set of electron energy loss spectroscopy measurements targeting *NO* and noted good agreement between their measurements and those of Chan *et al*. Figure 10a shows digitized data from Figs. 2 - 3 of Chan *et al* [24]. SPECAIR was found to predict the bound-bound transitions fairly accurately down to wavelengths of approximately 145 nm. It does not currently model the continuum that is seen in the measurements of Chan *et al*. If this continuum is manually added to the SPECAIR calculations, the resulting agreement with the cross-section measurements of Chan *et al* is shown in Fig. 10b. The bound-bound structure below 160 nm is almost entirely dominated by the β', $K - X$ and $Q - X$ systems of *NO*. In their paper, Chan *et al* report a spectral resolution FWHM of 0.048 eV for their measurements. However, they do not give the instrument lineshape function. Therefore, a Gaussian lineshape with a FWHM of 0.048 eV is assumed for the instrument function and applied this to the SPECAIR calculation. Because of this assumption, and also because the data was digitized from Chan *et al*, the comparison shown in Fig. 10b should be taken as indicative only.

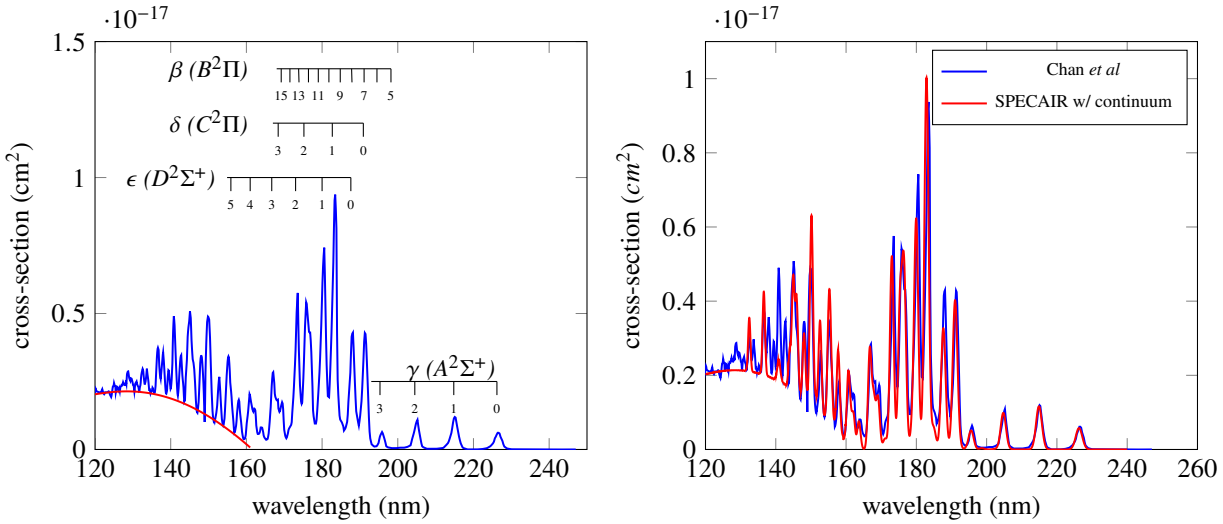

Fig. 10 a) Photoabsorption cross-sections measured by Chan *et al* (Figs. 2 - 3 of their paper) [24]. The red curve denotes the underlying continuum that is observed. b) Comparison between measurements of Chan *et al* and SPECAIR. The continuum shown in Fig. 10a has been manually added to the SPECAIR calculation.

Figures 10a and 10b suggest that there is a continuum source of emission/absorption from nitric oxide in the VUV.

To our knowledge, the source of this continuum has not been identified. In Fig. 10a, the underlying broadband structure appears to be from a true continuum, as opposed to a large broadening of spectral features such that they are merged together. If this is indeed the case, then inverse photodissociation would appear to be the culprit for the missing source - as opposed to pre-dissociation which would lead to a broadening and weakening of spectral features, but not to a broad continuum. The data reported by Chan *et al* was taken from nitric oxide at room temperature. Therefore, the reported cross-sections would have been measured from the ground electronic and ground vibrational level and would not allow us to account for vibrational excitation of the nitric oxide within the plasma jet studied in this work. However, to arrive at an order-of-magnitude estimation of the impact of the observed continuum on the spectrum from high temperature air as measured in the torch, these cross-sections were assumed to be independent of vibrational quantum number. In other words, the cross-sections are simply shifted by the energy of the particular excited vibrational level with respect to the ground vibrational level. This enabled an estimation of the emission that might be expected from the recombination $N + O \rightarrow NO$, if this is indeed the source of the observed continuum. Figure 11 shows the resulting comparison. The fairly good agreement suggests that such a continuum may indeed explain part or all of the observed discrepancy. Note that the overprediction of SPECAIR below 150 nm when accounting for this continuum is not necessarily problematic because a portion of the actual emitted signal could be absorbed by cold O_2 in the boundary of the plasma jet. Vibrationally specific photoabsorption cross-sections for NO, such as those presented for the O_2 molecule by Allison *et al* [33], would help in assessing this hypothesis.

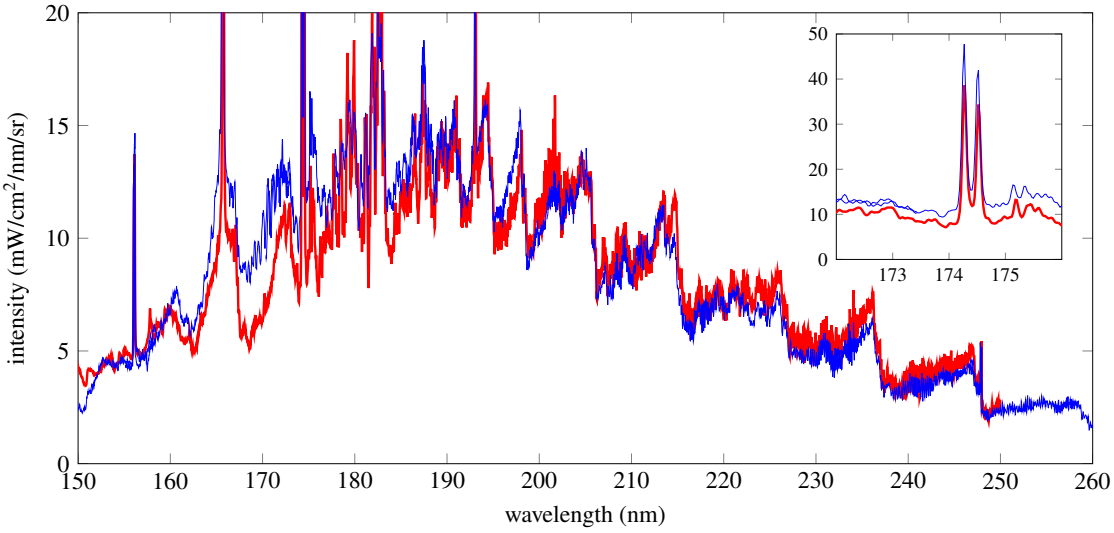

Fig. 11 Experiment and SPECAIR comparison - SPECAIR is red and experiment is blue. SPECAIR calculation includes estimate of continuum based upon Chan *et al* data [24].

B. Perturbations between the $^2\Sigma^+$ states of *NO*

A second potential candidate for the observed discrepancy would be additional excited state perturbations in the *NO* molecule not accounted for. De Vivie and Peyerimhoff [23] performed a comprehensive set of calculations with the goal of identifying and characterizing all electronic states of *NO* - including perturbations among the various states - up to the dissociation limit. They used a basis set composed of molecular and atomic orbitals in order to fully describe the molecular eigenstates and to calculate electronic transition dipole moments. They noted that their calculations are slightly less accurate than studies focused on a more limited subset of electronic states because of computational limitations. Indeed, the electronic transition dipole moment functions provided by De Vivie and Peyerimhoff are not used in SPECAIR calculations as other models were found to provide a better comparison with experimental data [7]. However, a big advantage of their calculation is the relatively complete picture that it provides of the various electronic states. They address the aforementioned perturbations among the various $^2\Pi$ states that were modeled by Gallusser and Dressler [25] and that are accounted for in SPECAIR. In addition, they also discuss perturbations among certain $^2\Sigma^+$ states. They note that the $A^2\Sigma^+$ and $D^2\Sigma^+$ (associated with the γ and ϵ molecular systems) interact with the $I^2\Sigma^+$ state and a second repulsive state that they label the $2^2\Sigma_v^+$ state (referred to as the $A'^2\Sigma^+$ state by Miescher [34]). These interactions lead to perturbations in the $v = 8$ vibrational level of $A^2\Sigma^+$ and $v = 3 - 4$ of $D^2\Sigma^+$. Figure 2 of the article by De Vivie and Peyerimhoff [23] shows the result of these perturbations on the electronic structure. A SPECAIR calculation of high temperature air emission (using the temperature profile in Fig. 2a) accounting only for the emission coming from these vibrational levels is shown in Fig. 12. These levels are responsible for a large portion of the emission at wavelengths between 160 and 180 nm where the discrepancy between calculation and experiment is largest (see Fig. 9b). Perturbations of these levels could therefore potentially account for the discrepancy seen with the measurements.

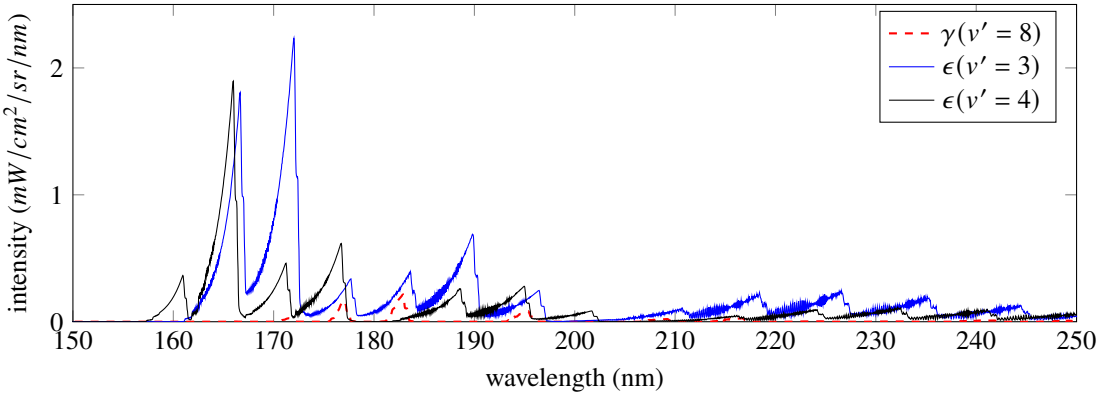

Fig. 12 Calculated emission from specific vibrational levels of the ϵ and γ systems of *NO* using the temperature profile in Fig. 2a.

VI. Conclusion

Measurements of high temperature air emission spectra between 150 - 250 nm (VUV/UV) are reported. This data is included with the article on the journal website - files containing the measured temperature profile, the slit function of the VUV spectrometer and the measured VUV spectrum are included. Subsequent comparisons with calculations led to several improvements in the SPECAIR radiation code, resulting in overall improved agreement. Perturbations amongst the various $^2\Pi$ states of *NO* were taken into account to better predict emission from the β and δ systems. Several other new molecular systems were also added. Finally, atomic line broadening was also taken into account as this was found to have a significant impact on the predicted intensity of the atomic nitrogen 174 nm line, namely because the emission from this atomic line is impacted by self-absorption. The overall agreement is considered to be good. Below 180 nm, the amplitude is underpredicted by SPECAIR, and the finer structure of the spectrum is not fully captured. With the improvements that were made, SPECAIR was also found to provide accurate predictions of photoabsorption data reported by Chan *et al* down to approximately 145 nm, with the exception of a continuum that becomes significant at wavelengths below 160 nm.

One possible explanation for the observed discrepancies between SPECAIR and the emission measurements is an unaccounted for continuum emission source. Though its source is unknown, order-of-magnitude estimates suggest that the continuum observed by Chan *et al* (red curve, Fig. 10a) could potentially explain the discrepancy between SPECAIR predictions and measurements below 180 nm. A second possible explanation could be linked to perturbations among the various $^2\Sigma^+$ states that are unaccounted for.

Acknowledgments

We would like to acknowledge the contributions of Umar A Sheikh, Richard Morgan and Victor Gondret who participated in the development of this VUV system. The VUV spectrometer was loaned to the authors by NASA Ames as part of an International NASA Space Act Agreement for equilibrium radiation measurements in collaboration with Brett Cruden of NASA Ames.

A. NO γ' ($E^2\Sigma^+$ - $X^2\Pi$) band system

Figure 13 shows how the inclusion of the γ' system impacts the cross-section calculation for comparison with the data of Chan *et al* as well as the calculation of the high temperature emission. This can be compared with Fig. 10b which does not include this system. Including this system adversely impacts the comparison with the data of Chan *et al* while having a negligible impact on the predicted emission from the plasma torch.

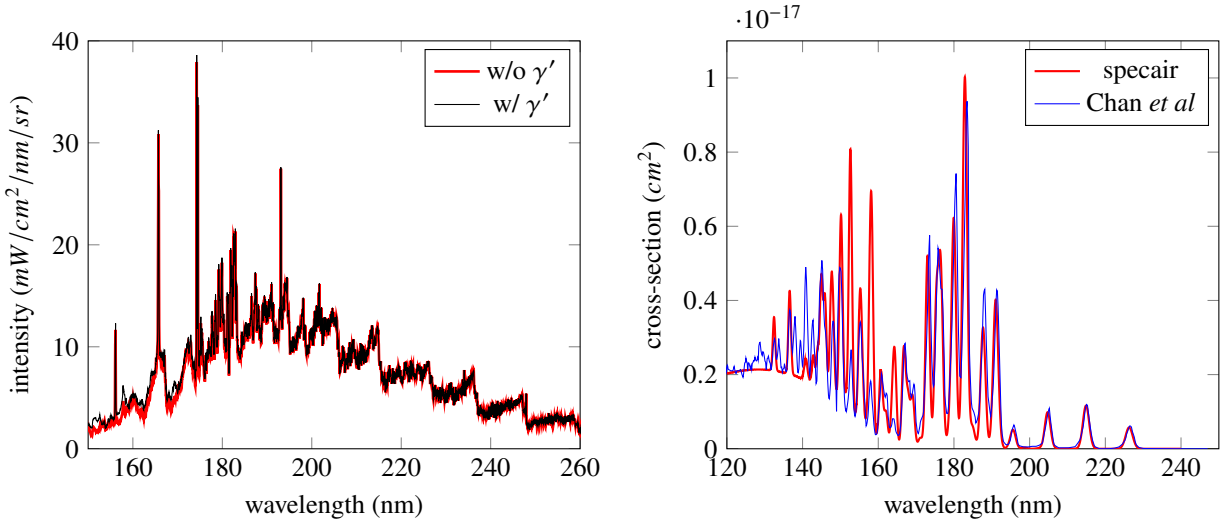

Fig. 13 a) SPECAIR calculations of high temperature air emission with (black) and without (red) the γ' system included. The red curve corresponds to the SPECAIR calculation in Fig. 9b. b) NO cross-section calculations including the γ' system in red are compared with the data of Chan *et al* in blue. The γ' transition results in an over-prediction of several features.

B. NO $F^2\Delta$ - $X^2\Pi$ band system

Two $Re(r)$ curves were tested for this system. Both were scaled to give the measured lifetime of the $v = 0$ level of the F-state reported by Brzozowski, Erman and Lyyra [35]. The first curve was simply a constant. The second was a scaled $Re(r)$ derived from the γ system. This second option was motivated by an observation that the $Re(r)$ curves used in SPECAIR for the $\gamma(A^2\Sigma^+ - X^2\Pi)$, $\epsilon(D^2\Sigma^+ - X^2\Pi)$ and $\delta(C^2\Pi - X^2\Pi)$ systems could be scaled by constants to produce a single curve - they appeared self-similar. Meanwhile, the potential energy curves for these states and the F-state have a similar form as well. Figure 14a shows how the different $Re(r)$ curves used affect the modeling of the F-X system cross-section calculation for *NO* at room temperature. Figure 14b shows how the full SPECAIR calculation compares with the measurements of Chan *et al* when accounting for the F-X system. Figure 15 shows how the inclusion of the F-X system impacts the SPECAIR prediction of the emission from the plasma torch. The inclusion of the F-X system adversely impacts the comparison with the data of Chan et al while having a negligible impact on the predicted emission from the plasma torch.

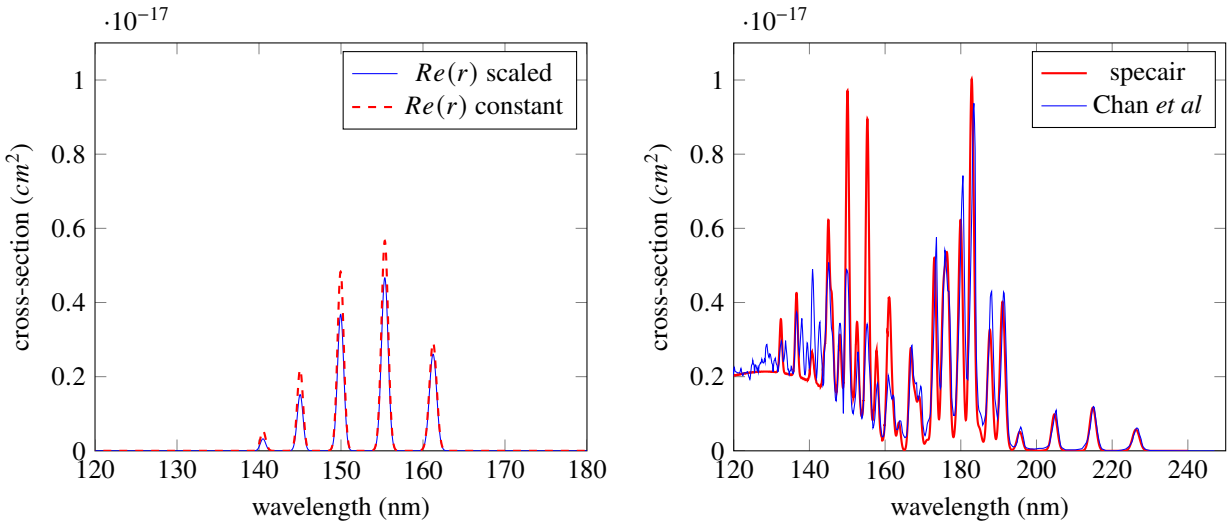

Fig. 14 **a) Comparison between SPECAIR calculations of the F-X absorption cross-sections using a constant $Re(r)$ or an $Re(r)$ self-similar to that of the *NO* γ system. In both cases, the $Re(r)$ curve has been scaled so that the lifetime of the $v' = 0$ level matches the lifetime reported by Brzozowski *et al* [35]. In the calculations/figures to follow, the scaled $Re(r)$ curve was used for F-X calculations. b) NO cross-section calculations including the $F - X$ system in red are compared with the data of Chan *et al* in blue.**

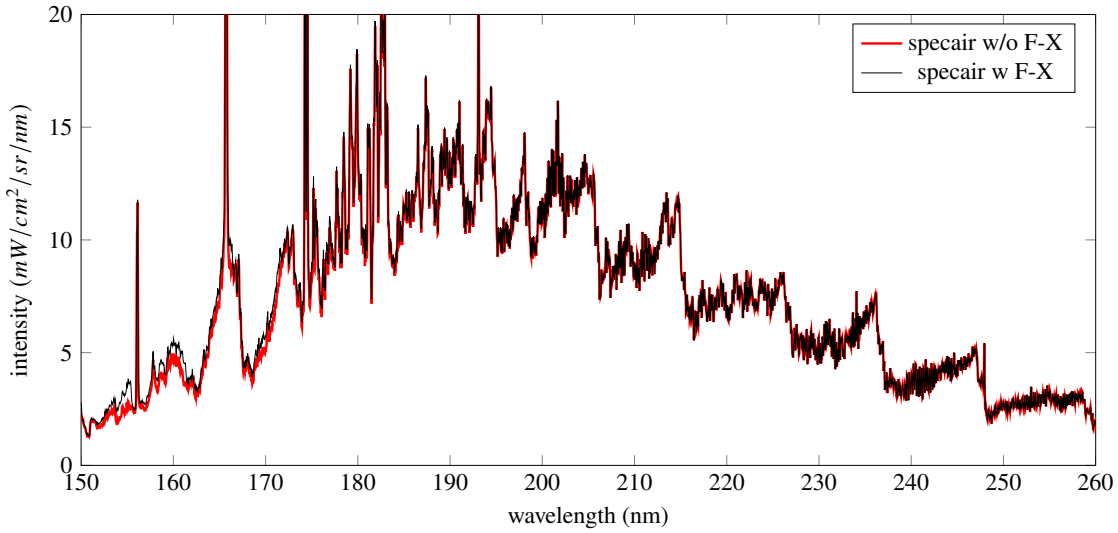

Fig. 15 **SPECAIR calculation of line-of-sight emission with the temperature profile in Fig. 2a. The red curve corresponds to the SPECAIR calculation in Fig. 9b. The black curve includes the *NO* F-X system.**

References

[1] Griem, H., *Principles of Plasma Spectroscopy*, Cambridge University Press, 1997.

[2] Johnston, C. O., Mazaheri, A., Gnoffo, P., Kleb, B., and Bose, D., "Radiative Heating Uncertainty for Hyperbolic Earth Entry, Part 1: Flight Simulation Modeling and Uncertainty," 2013, pp. 19–38. https://doi.org/10.2514/1.A32254.

[3] Laux, C., Winter, M., Merrifield, J., Smith, A., and Tran, P., "Influence of Ablation Products on the Radiation at the Surface of a Blunt Hypersonic Vehicle at 10 km/s," *41st AIAA Thermophysics Conference*, 2009. https://doi.org/10.2514/6.2009-3925.

[4] Zammit, M. C., Leiding, J. A., Colgan, J., Even, W., Fontes, C. J., and Timmermans, E., "A comprehensive study of the radiative properties of NO—a first step toward a complete air opacity," *Journal of Physics B: Atomic, Molecular and Optical Physics*, Vol. 55, No. 18, 2022, p. 184002. https://doi.org/10.1088/1361-6455/ac8213, URL https://dx.doi.org/10.1088/1361-6455/ac8213.

[5] Laux, C. O., Spence, T. G., Kruger, C. H., and Zare, R. N., "Optical diagnostics of atmospheric pressure air plasmas," *Plasma Sources Science and Technology*, Vol. 12, No. 2, 2003, p. 125. URL https://iopscience.iop.org/article/10.1088/0963-0252/12/2/301.

[6] "SPECAIR, Software Package, Ver. 3.0, SpectralFit S.A.S." , 2012. URL http://www.spectralfit.com.

[7] Laux, C., "Optical Diagnostics and Radiative Emission of Air Plasmas," Ph.D. thesis, Stanford University, Dept. of Mechanical Engineering, 1993.

[8] MacDonald, M., Jacobs, C., Laux, C., Zander, F., and Morgan, R., "Measurements of Air Plasma/Ablator Interactions in an Inductively Coupled Plasma Torch," *Journal of Thermophysics and Heat Transfer*, Vol. 29, No. 1, 2014, pp. 12–23. https://doi.org/10.2514/1.T4402.

[9] McBride, B. J., and Gordon, S., "Computer Program for Calculating and Fitting Thermodynamic Functions," Tech. rep., NASA RP-1271, 1992.

[10] Jacobs, C., Sheikh, U. A., MacDonald, M., and Laux, C. O., "Vacuum ultraviolet radiation studies in a plasma torch facility," *44th AIAA Thermophysics Conference*, 2013. https://doi.org/10.2514/6.2013-3015.

[11] McGuire, S. D., Tibère-Inglesse, A. C., Mariotto, P. B., Cruden, B. A., and Laux, C. O., "Measurements and modeling of CO 4th positive (A–X) radiation," *Journal of Quantitative Spectroscopy and Radiative Transfer*, Vol. 245, 2020, p. 106855. https://doi.org/10.1016/j.jqsrt.2020.106855.

[12] Tibère-Inglesse, A. C., McGuire, S. D., Mariotto, P., and Laux, C. O., "Experimental study of recombining nitrogen plasmas: II. Electronic population distributions and nonequilibrium radiation of atoms," *Plasma Sources Science and Technology*, Vol. 30, No. 12, 2021, p. 125020. https://doi.org/10.1088/1361-6595/ac2221.

[13] Klose, J., Bridges, J., and Ott, W., "Radiometric Calibrations of Portable Sources in the Vacuum Ultraviolet," *Journal of Research of the National Bureau of Standards*, Vol. 93, No. 1, 1988, pp. 21–39.

[14] Laux, C., and Kruger, C., "Arrays of radiative transition probabilities for the N_2 first and second positive, NO beta and gamma, N_2^+ first negative, and O_2 Schumann-Runge band systems," *Journal of Quantitative Spectroscopy and Radiative Transfer*, Vol. 48, No. 1, 1992, pp. 9 – 24. https://doi.org/10.1016/0022-4073(92)90003-M.

[15] Laux, C., Gessman, R., and Kruger, C., "Modeling the UV and VUV radiative emission of high-temperature air," 1993. https://doi.org/10.2514/6.1993-2802.

[16] Schadee, A., "Unique definitions for the band strength and the electronic-vibrational dipole moment of diatomic molecular radiative transitions," *Journal of Quantitative Spectroscopy and Radiative Transfer*, Vol. 19, No. 4, 1978, pp. 451 – 453. https://doi.org/10.1016/0022-4073(78)90120-6.

[17] Whiting, E., Schadee, A., Tatum, J., Hougen, J., and Nicholls, R., "Recommended conventions for defining transition moments and intensity factors in diatomic molecular spectra," *Journal of Molecular Spectroscopy*, Vol. 80, No. 2, 1980, pp. 249 – 256. https://doi.org/10.1016/0022-2852(80)90137-X.

[18] Amiot, C., "The infrared emission spectrum of NO: Analysis of the Δv = 3 sequence up to v = 22," *Journal of Molecular Spectroscopy*, Vol. 94, No. 1, 1982, pp. 150–172. https://doi.org/10.1016/0022-2852(82)90301-0.

[19] Lavrov, B., "Calculation of Thermodynamic Functions for N_2, O_2 and NO," *SUDAAR*, Stanford University, 1991.

[20] Huber, K., and Herzberg, G., *Molecular spectra and Molecular Structure. IV. Constants of diatomic molecules.*, Van-Nostrand-Reinhold, 1979.

[21] Langhoff, S. R., Bauschlicher, C. W., and Partridge, H., "Theoretical study of the NO γ system," *The Journal of Chemical Physics*, Vol. 89, No. 8, 1988, pp. 4909–4917. https://doi.org/10.1063/1.455661.

[22] Sheehy, J. A., Bauschlicher, C. W., Langhoff, S. R., and Partridge, H., "Theoretical study of the nitric oxide ϵ and 11000 Å bands," *Chemical Physics Letters*, Vol. 225, No. 1, 1994, pp. 221–228. https://doi.org/10.1016/0009-2614(94)00608-3.

[23] de Vivie, R., and Peyerimhoff, S. D., "Theoretical spectroscopy of the NO radical. I. Potential curves and lifetimes of excited states," *The Journal of Chemical Physics*, Vol. 89, No. 5, 1988, pp. 3028–3043. https://doi.org/10.1063/1.454958.

[24] Chan, W., Cooper, G., and Brion, C., "Absolute optical oscillator strengths for the photoabsorption of nitric oxide (5–30 eV) at high resolution," *Chemical Physics*, Vol. 170, No. 1, 1993, pp. 111–121. https://doi.org/10.1016/0301-0104(93)80097-S.

[25] Gallusser, R., and Dressler, K., "Multistate vibronic coupling between the excited $^2\Pi$ states of the NO molecule," *The Journal of Chemical Physics*, Vol. 76, No. 9, 1982, pp. 4311–4327. https://doi.org/10.1063/1.443565.

[26] Qu, Q., Cooper, B., Yurchenko, S. N., and Tennyson, J., "A spectroscopic model for the low-lying electronic states of NO," *The Journal of Chemical Physics*, Vol. 154, No. 7, 2021, p. 074112. https://doi.org/10.1063/5.0038527.

[27] Amiot, C., and Verges, J., "Fine Structure of the $C^2\Pi$-$A^2\Sigma^+$ and $D^2\Sigma^+$-$A^2\Sigma^+$ Band Systems of the NO Molecule: Homogeneous and Heterogeneous Perturbations," *Physica Scripta*, Vol. 25, No. 2, 1982, pp. 302–311. https://doi.org/10.1088/0031-8949/25/2/009.

[28] Imajo, T., Yoshino, K., Esmond, J. R., Parkinson, W. H., Thorne, A. P., Murray, J. E., Learner, R. C. M., Cox, G., Cheung, A. S.-C., Ito, K., and Matsui, T., "The application of a VUV Fourier transform spectrometer and synchrotron radiation source to measurements of: II. The $\delta(1,0)$ band of NO," *The Journal of Chemical Physics*, Vol. 112, No. 5, 2000, pp. 2251–2257. https://doi.org/10.1063/1.480790.

[29] Partridge, H., Langhoff, S. R., and Bauschlicher, C. W., "Theoretical study of the spectroscopy of NO+," *The Journal of Chemical Physics*, Vol. 93, No. 10, 1990, pp. 7179–7186. https://doi.org/10.1063/1.459716.

[30] Pilling, M., Bass, A., and Braun, W., "A curve of growth determination of the f-values for the fourth positive system of CO and the Lyman-Birge-Hopfield system of N2," *Journal of Quantitative Spectroscopy and Radiative Transfer*, Vol. 11, No. 11, 1971, pp. 1593–1604. https://doi.org/10.1016/0022-4073(71)90137-3.

[31] Griem, H., *Spectral Line Broadening by Plasmas*, Academic Press, 1974.

[32] Kato, H., Kawahara, H., Hoshino, M., Tanaka, H., and Brunger, M., "Excitation of the $A^2\Sigma^+$, $C^2\Pi$ and $D^2\Sigma^+$ Rydberg-electronic states in NO by 100eV electrons," *Chemical Physics Letters*, Vol. 444, No. 1, 2007, pp. 34–38. https://doi.org/10.1016/j.cplett.2007.06.134.

[33] Allison, A., Dalgarno, A., and Pasachoff, N., "Absorption by vibrationally excited molecular oxygen in the Schumann-Runge continuum," *Planetary and Space Science*, Vol. 19, No. 11, 1971, pp. 1463–1473. https://doi.org/10.1016/0032-0633(71)90007-9.

[34] Miescher, E., "The $I^2\Sigma^+$ state of the *NO* molecule," *Journal of Molecular Spectroscopy*, Vol. 69, No. 2, 1978, pp. 281–293. https://doi.org/10.1016/0022-2852(78)90065-6.

[35] Brzozowski, J., Erman, P., and Lyyra, M., "Predissociation Rates and Perturbations of the A, B, B', C, D and F States in NO Studied Using Time Resolved Spectroscopy," *Physica Scripta*, Vol. 14, No. 6, 1976, pp. 290–297. https://doi.org/10.1088/0031-8949/14/6/009.